

Ethyne Adsorbed on CuNaY Zeolite: FTIR Spectra and Quantum Chemical Calculations

Georg Hübner,[†] Guntram Rauhut,[‡] Hermann Stoll,[‡] and Emil Roduner^{*,†}*Institutes of Physical Chemistry and Theoretical Chemistry, University of Stuttgart, Pfaffenwaldring 55, 70569 Stuttgart, Germany**Received: February 5, 2003; In Final Form: May 29, 2003*

The interaction of ethyne with vacuum-dehydrated CuNaY zeolite has been investigated by means of Fourier transform infrared spectroscopy and cluster model density functional theory calculations. The spectra show three bands: two which are symmetry-forbidden for the free molecule but become allowed in the adsorbed state (the ν_1 CC stretching mode at ~ 1832 and 1814 – 1812 cm^{-1} , and the symmetric ν_2 CH stretching mode at 3271 and 3251 cm^{-1}), and the allowed antisymmetric ν_3 CH stretching mode at 3202 and 3174 cm^{-1} . They all appear in pairs. The two components of the bands, which are all strongly shifted to lower wavenumbers relative to the free molecule, are attributed to two inequivalent Cu^+ adsorption sites. On increasing C_2H_2 pressure, the more strongly shifted components appear first and acquire significantly higher intensity, indicating that they must correspond to the more strongly bound site. Analysis of the geometry of the complexes representing ethyne adsorbed on Cu at both sites yields a four-fold coordination of copper, including two oxygen atoms and side-on bound C_2H_2 , with CC bonds elongated by 0.03 Å and CCH angles reduced by at least 14.7° . The calculated binding energies of the two ethyne–copper complexes are significantly different due to the energy necessary to reach the geometry within $\text{Cu}(\text{SII})-\text{C}_2\text{H}_2$ from the relaxed $\text{Cu}(\text{SII})$ cluster. C_2H_2 is more strongly adsorbed on $\text{Cu}(\text{SIII})$ (in the saddle between two four-membered rings near the wall of a supercage) than on site II (above a six-ring window of a sodalite cage). Population analysis provides a net charge transfer of about $0.14e$ toward the ethyne. An energy decomposition method demonstrates the paramount importance of electrostatic and charge-transfer contributions to the Cu–zeolite–ethyne interaction energy. The harmonic frequency calculation suggests that the more strongly shifted band components of all stretching vibrations have to be assigned to C_2H_2 adsorbed on Cu^+ at SIII, which is the more stable site. Apart from the overestimated $\Delta\nu_1$ values, the vibrational frequency shifts calculated for both adsorption complexes are in excellent agreement with the experimental ones.

1. Introduction

Microporous materials containing transition metals are of fundamental interest and also of practical importance due to their high catalytic activity and selectivity in various industrial processes. Copper-exchanged zeolites, to which our main concern is dedicated, are active substrates for the decomposition of N_2O and NO into N_2 and O_2 .^{1–4} Especially overexchanged Cu–ZSM-5 zeolites with high Si/Al ratios show high catalytic NO decomposition activity, suggesting the existence of neighboring copper centers interacting with the N–N bond because of their favorable geometric arrangement within the framework.⁵

Some organic reactions, such as the Diels–Alder cyclodimerization of 1,3-butadiene to vinylcyclohexene^{6–9} or the coupling reaction of ethyne and 1,3-butadiene to 1,4-cyclohexadiene,^{6,8} are likewise worthy of mention. They can be carried out under mild conditions using copper-containing zeolites. It seems that the presence of Cu^+ ions within the zeolites, generated via mild reduction of Cu^{2+} ions^{6–8} or direct exchange with CuI in liquid ammonia,⁸ and certain spatial conditions enforced by the framework have a substantial beneficial effect on these transformations.

The potential cation sites in faujasites are well known.¹⁰ To facilitate further discussion, these sites are shown in Figure 1,

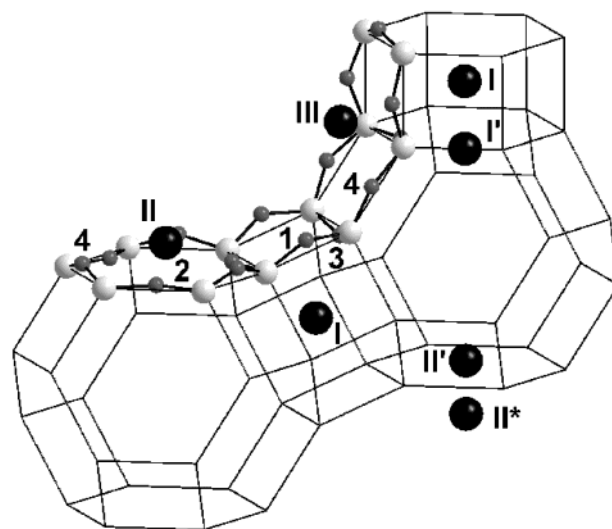


Figure 1. Structural fragment of zeolite Y. The lines represent the aluminosilicate framework, with Si and Al atoms (light gray) sitting at the vertexes, separated by one oxygen atom (dark gray) near the interconnecting line. The four inequivalent oxygen sites are labeled by arabic numbers. The cation positions are given by heavy black balls and marked by roman numerals. For clarity, the topology around the cation positions SII and SIII is given in detail.

with emphasis on the topology around the cations of sites II and III, which is of interest in the present context. Cu^{2+} ions

* To whom correspondence should be addressed. E-mail: e.roduner@ipc.uni-stuttgart.de.

[†] Institute of Physical Chemistry.

[‡] Institute of Theoretical Chemistry.

incorporated into NaY zeolite are reduced to Cu^+ by intrazeolitic water¹¹ or framework oxygen¹² during heat treatment under vacuum. Several techniques revealed two reduction processes of Cu^{2+} ions on sodalite and supercage sites,¹¹ and residual, paramagnetic Cu^{2+} ions were located at sites I and/or I' by electron spin resonance spectroscopy.¹³ A ^{129}Xe NMR study by Hartmann and Boddenberg identified two inequivalent Cu(I) ions besides unexchanged Na^+ ions: Lewis and Brønsted sites arising from the dehydration, and unoccupied framework sites accessible to the probes, i.e., within the supercage.¹⁴ Large probe molecules such as ethyne can access only sites within the supercage. Among these sites, the ones with the largest fractional occupancy in copper-exchanged NaY are SII and SIII,¹⁵ thus, only these sites were considered in the present study.

Ethyne, the simplest alkyne, is able to bind to surface sites by virtue of either its terminal hydrogen atoms or the central CC triple bond. The acidic character of the CH groups favors the interaction with basic sites via H-bonding, as was demonstrated by the shifts to lower wavenumbers of the antisymmetric CH stretching vibrations of ethyne adsorbed on MgO ¹⁶ and on the alkali-exchanged zeolites NaY and CsNaY.¹⁷ The triple bond, however, is primarily involved in the formation of π -complexes (*side-on* or η^2 -coordination) with acidic bridging OH groups^{18,19} and with Lewis sites such as Na^+ ions of a Y¹⁷ or A²⁰ zeolite. As is already well known from studies of organometallic compounds, there are also a few examples of π adducts consisting of metal cations and ethyne, e.g., the $\text{Cd}^{2+}-(\eta^2\text{-C}_2\text{H}_2)$ ²¹ and the $\text{Ni}^{2+}-(\eta^2\text{-C}_2\text{H}_2)$ complexes²² on X and Y zeolite, which were explored by neutron scattering and single-crystal X-ray diffraction, respectively. To interpret some of the experimental results, quantum chemical calculations at the density functional theory (DFT) or second-order Møller–Plesset perturbation theory (MP2) level were performed using restricted clusters^{23–25} as well as periodic systems²⁶ to mimic the zeolite or selected fragments thereof and their interaction with ethyne. As expected, ethyne is side-on bound on top of Si–OH and bridged Si–OH–Al groups, with $\text{H}\cdots\text{C}$ bond distances ranging from 2.34 to 2.38 Å and from 2.17 to 2.27 Å.^{24,25} The same coordination is found for the radical anion of C_2H_2 , which is formed in the cis-bent configuration upon the radiolysis of ethyne-loaded H–ZSM-5, as could be demonstrated by the combined electron spin resonance and theoretical study of Picos et al.²⁷ Due to the interaction with the acidic proton of bridging OH groups, the CC bond length of C_2H_2 is only very slightly elongated by ≤ 0.003 Å (B3LYP/6-31G** and MP2/DZP levels).^{24,25} On the basis of Mulliken atomic charges (SCF/DZP level), a small electron transfer of 0.02 electron from the adsorbed ethyne toward the acidic zeolite was predicted by Ugliengo et al.²⁴ Nevertheless, these authors denote the nature of the interaction as predominantly electrostatic.²⁴ If explicitly assigned, the calculated harmonic frequency shifts of the CC stretching mode amount to -9 (MP2/DZP)^{24,25} and -15 cm^{-1} (B3LYP/6-31G**),²⁵ compared to the experimental value of -24 cm^{-1} . With regard to the interaction with Lewis sites, modeled quite simply by adducts consisting of bare cations, as Li^+ , Na^+ , K^+ , Cs^+ , and Ni^{2+} , the recent ab initio study by Garrone et al.²⁸ and the B3LYP investigations of Catlow and co-workers²² unambiguously confirm that ethyne is bound side-on as well. The largest shift to lower wavenumbers of the CC stretching mode with respect to the value in the gas phase amounts to -29 cm^{-1} and was calculated for C_2H_2 interacting with one Li^+ ion.²⁸

This paper extends our previous study concerning ethene and its ability to discriminate between two inequivalent Cu(I) sites

with vacuum-dehydrated CuNaY zeolite.²⁹ Motivated by the properties of ethyne, which can act as both a Brønsted acid and a Lewis base, depending on the character of the molecular environment, and encouraged by its simple structure, we examine Fourier transform infrared (FTIR) spectra of ethyne on CuNaY zeolite. In the context of the experimental work, it has to be clarified whether C_2H_2 is bound to the acidic proton of bridging OH groups, to residual sodium ions, or the Cu(I) sites, and what the geometry at the binding site is. Additionally, the questions of to what extent this geometry resembles that of ethene and whether C_2H_2 behaves in a comparable fashion have to be answered. To support the assignments derived from FTIR spectra, we present quantum chemical calculations on the basis of two models mimicking Cu^+ ions on sites II and III within the cluster approach. The theoretical work consists of geometry optimizations and harmonic frequency calculations of the corresponding ethyne adsorption complexes and their interaction energies, using the B3LYP functional, and is completed by natural atomic orbital/natural bond orbital (NAO/NBO) analysis as well as energy decomposition methods at the uncorrelated (reduced variational space, RVS) and correlated levels (local second-order Møller–Plesset perturbation theory, LMP2).

2. Computational Section

Density functional calculations, using the B3LYP³⁰ exchange-correlation functional as implemented in GAUSSIAN 98, were performed for geometry optimizations and frequency calculations.³¹ For detailed information concerning the zeolite model clusters, the pseudopotentials, the atomic basis sets, and the geometry optimization procedure, as well as the harmonic frequency calculations, we refer the reader to ref 29.

To reveal the nature of the $\text{C}_2\text{H}_2\text{--Cu}^+$ bonds within the adsorption complexes, we performed NAO/NBO analysis, developed by Weinhold et al., as implemented in GAUSSIAN 98.^{32,33} The RVS method^{34,35} at the restricted Hartree–Fock level and the LMP2 correlation energy decomposition,³⁶ both contained in the ab initio program packages GAMESS³⁷ and MOLPRO,³⁸ were used to analyze quantitatively the different contributions to the electronic interaction energies between the monomeric parts (see ref 29 for further explanations).

3. Experimental Section

CuNaY was prepared from NaY zeolite (CU Chemie Uetikon AG) as described previously.³⁹ A Cu exchange level of 64% was determined by inductively coupled plasma atomic emission spectroscopy (ICP/AES). Activation of the zeolite wafers was done in situ at 673 K under high vacuum for at least 16 h. Transmission FTIR spectra were collected on a Nicolet Magna 560 spectrometer using a resolution of 2 cm^{-1} and 256 scans. Difference spectra of C_2H_2 with respect to the dehydrated zeolite were recorded during all experiments.

4. Results and Discussion

4.1. Experimental Results. Figure 2 shows the FTIR transmission spectra of ethyne adsorbed on vacuum-dehydrated CuNaY in the CH (left side) and CC stretching regions (right side) as a function of the loading. The bands are assigned following Herzberg to ν_1 , ν_2 , and ν_3 .⁴⁰ The experimental frequencies, the calculated harmonic frequencies, and the frequency shifts of C_2H_2 in the gas phase and adsorbed on two different copper sites are compared in Table 1.

The spectra reveal that all three absorption bands appear in pairs, with a high-intensity feature at lower frequency and a

TABLE 1: Comparison of the Experimental and Calculated Harmonic Frequencies (ν) and Frequency Shifts ($\Delta\nu$, in cm^{-1}) of Ethyne in the Gas Phase and Adsorbed at Two Different Copper Positions (Named Cu(SII) and Cu(SIII) Clusters in the Calculations)^a

no. ^b	C ₂ H ₂ (g)				Cu(SII)–C ₂ H ₂		Cu(SIII)–C ₂ H ₂	
	ν_{exp}^c	sym ^d /act	mode ^e	ν_{calc}	$\Delta\nu_{\text{exp}}$	$\Delta\nu_{\text{calc}}$	$\Delta\nu_{\text{exp}}$	$\Delta\nu_{\text{calc}}$
ν_1	1974	Σ_g^-/RE	CC str	2075	−142 ^f	−182	−160 to −162 ^{f,g}	−190
ν_2	3373	Σ_g^-/RE	CH s str	3529	−102 ^f	−106	−122 ^f	−116
ν_3	3282	Σ_u^-/IR	CH as str	3427	−80 ^f	−84	−108 ^f	−93

^a All frequencies and frequency shifts were *not* scaled. ^b Numbering following Herzberg.⁴⁰ ^c Experimental frequencies taken from refs 40 and 43. ^d Symmetry species and vibrational activities (IR and RE) for gaseous C₂H₂ belonging to the $D_{\infty h}$ point group ($z \parallel \text{HCCH}$ axis). ^e Approximate description of the normal modes. s and a are related to the symmetry regarding the σ_h mirror plane. ^f Assignment supported by correlation with increasing equilibrium pressures of ethyne (hf and lf components of ν_1 , ν_2 , and ν_3 bands, respectively; see Figure 2). ^g Small variations of the frequency with increasing loading.

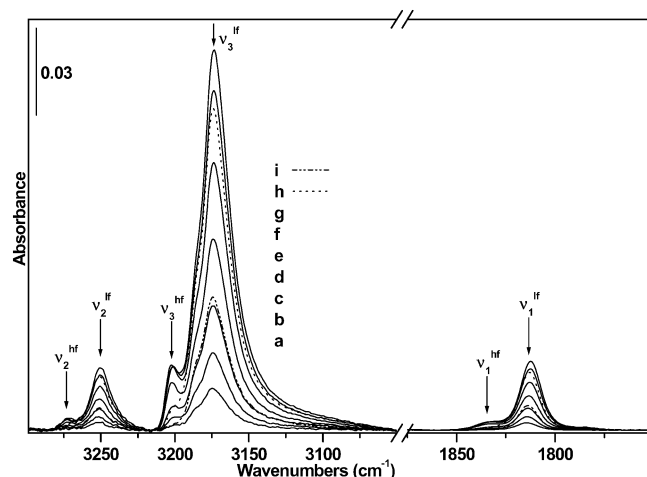


Figure 2. FTIR transmission spectra of C₂H₂ on CuNaY at 298 K in the CH and the CC stretching regions after adsorption of C₂H₂ on CuNaY at 298 K and equilibrium pressures of (a) 0.17, (b) 0.34, (c) 0.51, (d) 1.0, (e) 2.7, (f) 5.3, and (g) 10.1 hPa. The peak intensities grow with increasing pressure from (a) to (g). The spectra (h) and (i) were recorded after evacuation for ~1 and ~65 h, respectively.

minor feature at higher frequency. In the following, we will refer to these pairs by pairs of wavenumbers, separated by a slash, and the corresponding low-/high-frequency components will be designated with “lf”/“hf” superscripts, respectively. The bands in Figure 1 are centered at 3271/3251 cm^{-1} (attributed to the symmetric CH stretching vibration, $\nu_2^{\text{hf}}/\nu_2^{\text{lf}}$), at 3202/3174 cm^{-1} (the antisymmetric CH stretching vibration, $\nu_3^{\text{hf}}/\nu_3^{\text{lf}}$), and at ~1832/1814–1812 cm^{-1} (the CC stretching mode, $\nu_1^{\text{hf}}/\nu_1^{\text{lf}}$). The low-frequency component of the ν_3 band, ν_3^{lf} , additionally shows a shoulder at ~3186 cm^{-1} and an extended absorption tail between ~3150 and ~3050 cm^{-1} . These minor spectral features might be tentatively assigned to the varying aluminum distribution of the zeolite framework influencing the properties of the cation sites and thus the vibrational frequencies of the adsorbed ethyne, but an in-depth study of these aspects is beyond the scope of the present work.

The seven normal modes of gaseous ethyne represent three stretching vibrations along the z axis ($\nu_1(\Sigma_g^-)$, $\nu_2(\Sigma_g^-)$, and $\nu_3(\Sigma_u^-)$), and the two two-fold degenerate bending vibrations perpendicular to the molecular axis ($\nu_4(\Pi_g)$ and $\nu_5(\Pi_u)$). The exclusion rule allows one to derive the Raman activity of all modes which are symmetric to the inversion center (*gerade* symmetry), while the other modes are IR active (*ungerade* symmetry). Consequently, the ν_1 and ν_2 modes of C₂H₂ are IR-inactive for the free molecule and activated due to adsorption in the anisotropic environment of a zeolite. Hence, the inhomogeneous electric field generated by the microporous material acts on the charge distribution of the ethyne and lowers its

symmetry; i.e., the inversion symmetry is broken. As pointed out by de Lara,²⁰ the shifts to lower wavenumbers of the ν_1 , ν_2 , and ν_3 modes, with transition dipole moments lying along the molecular axis, demonstrate that C₂H₂ is oriented perpendicularly to the electric field of the zeolite. The bending vibrations ν_4 and ν_5 , which should be shifted to higher wavenumbers following the rule of de Lara, could not be resolved. They are most probably masked by highly intense vibrations of the zeolitic framework.

In each pair of the three stretching vibrations in Figure 2, the component which is more strongly shifted to lower wavenumbers, “lf”, unambiguously appears first when the equilibrium pressure of C₂H₂ is increased. The ethyne corresponding to the “hf” components can be almost completely removed on evacuation. Furthermore, there are clear correlations between all “hf” and “lf” components as a function of the loading. Analogous findings are already known from the spectra of ethene on CuNaY²⁹ and can be explained exclusively by the existence of two chemically inequivalent adsorption sites, identified as Cu(I) ions due to the large shifts to lower wavenumbers of the CC stretching mode of ethyne. This assignment is supported by the absence of π -adducts between C₂H₂ and acidic bridging OH groups^{18,25} or Na⁺ ions of the zeolites Y¹⁷ and A,²⁰ which are expected at 1950 cm^{-1} or at 1958 and 1945 cm^{-1} . H-bonded ethyne complexes, detectable on basic sites in NaY and cesium-exchanged NaY zeolites¹⁷ and on MgO,¹⁶ can be excluded as well. This has to be anticipated due to the autoreduction process generating Brønsted acidic sites, as evidenced by temperature-programmed reduction (TPR) techniques¹¹ and FTIR spectroscopy by Hübner and Roduner.³⁹ The dramatic shift to lower wavenumbers of the CC stretching mode strongly supports the well-known side-on coordination of C₂H₂ to the metal center (see ref 29). Further analysis of the adsorption complexes, the prevailing chemical bonds, and the vibrations of ethyne are subjects of the computational part, below.

4.2. Computational Results. 4.2.1. Geometries. High-level quantum chemical calculations are affordable only for fragments of limited size. As in our previous work,²⁹ we chose the minimal clusters consisting of five silicon, one aluminum, and six oxygen atoms forming the six-membered ring of SII or the double four-membered ring of SIII (compare Figure 1). Dangling bonds were saturated by hydrogen atoms. Geometry optimization was conducted with the silicon and aluminum atoms fixed at their crystallographic lattice positions in order to simulate the constraints imposed by the framework. The suitability of this procedure was justified in ref 29, where also the structures of the bare clusters were given in detail.

The partially optimized geometries of the Cu(SII)–C₂H₂ and the Cu(SIII)–C₂H₂ adsorption complexes are depicted in Figure 3. Adsorption of ethyne at site II influences dramatically the geometry around the Cu⁺ cation. In close analogy to the

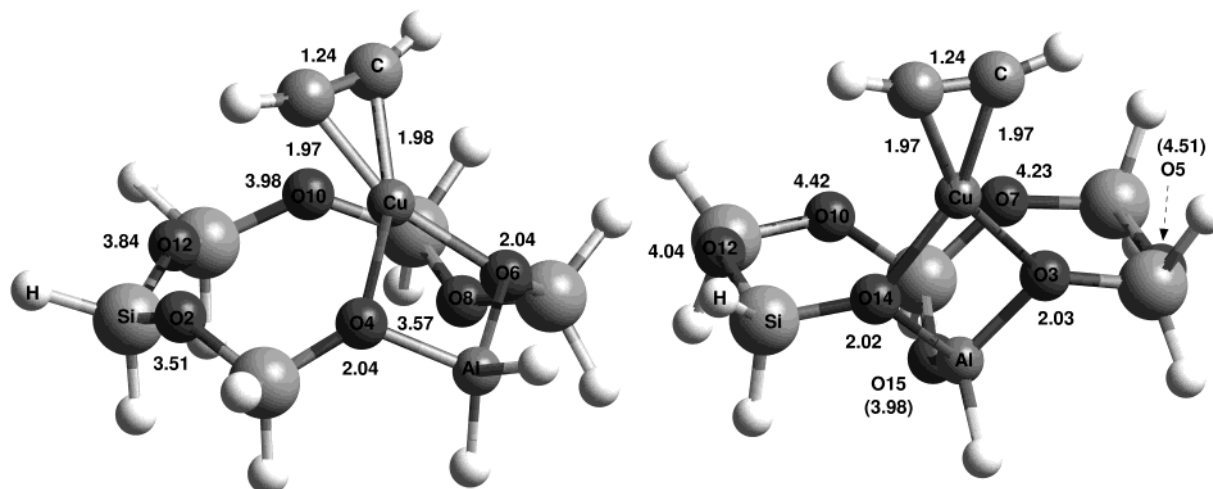


Figure 3. Optimized geometries of the Cu(II)–C₂H₂ (left) and the Cu(III)–C₂H₂ (right) adsorption complex. The Cu–O distances, in Å, are indicated at the oxygen atoms. All other distances are marked at the corresponding bonds.

TABLE 2: Calculated Interaction Energies for the Cu(II)–C₂H₂ and Cu(III)–C₂H₂ Complexes at the B3LYP Level (Values in kJ·mol^{−1})

	Cu(II)–C ₂ H ₂		Cu(III)–C ₂ H ₂	
	relaxed ^a	unrelaxed ^b	relaxed	unrelaxed
ΔE^c	−94	−171	−154	−180
BSSE ^d		−10		−11
ΔE_{BSSE}^e	−84	−161	−143	−169

^a Relaxation with respect to the corresponding monomers. ^b No relaxation. ^c Interaction energies without correction for the basis set superposition error (BSSE). ^d Counterpoise (CP) correction⁴¹ to account for the BSSE. ^e CP-corrected interaction energies.

formation of the Cu(II)–C₂H₄ complex,²⁹ the geometry changes to a nearly planar, four-fold coordination of the metal ion by two oxygen atoms (O4 and O6) and side-on bound C₂H₂ at a distance of 2.04 Å (2 × Cu–O) and 1.97/1.98 Å (2 × Cu–C). The C–C bond is elongated by 0.03 Å to 1.24 Å. Both C–C–H angles are distinctly reduced, with a mean value of 164.3°.

In contrast, C₂H₂ adsorption on the Cu(III) cluster merely results in slight variations of the structure. Here, the Cu⁺ ion is equally coordinated by two oxygen ligands, O3 and O14, and ethyne at distances of 2.03/2.02 Å and 1.97 Å (2 × Cu–C), respectively. The C–C bond distance of the ethyne amounts to 1.24 Å, and the C–C–H angles are 163.3° on average. Thus, while the local environment of the copper ion on the two sites is quite different in the bare clusters, it is nearly equivalent after ethyne adsorption.

Compared to ethene in the adsorbed state,²⁹ the Cu–C bond length is further reduced by approximately 0.05 Å. Concerning the CC triple bond, the elongation of 0.03 Å amounts to about half the value of ethene. However, the angular distortion, i.e., the reduction of the C–C–H angles with respect to the linear molecule, of 16.2° is clearly more pronounced as compared to the half-angle measured between the two CH₂ planes of the ethene complexes, which amounts to 11.6° on average. The C₂H₂···Cu fragment therefore resembles the metallocyclopropene complexes known from organometallic compounds.

4.2.2. Cu–Zeolite–Ethyne Energy Decomposition. Table 2 shows the calculated interaction energies of the complexes Cu(II)–C₂H₂ and Cu(III)–C₂H₂ at the B3LYP level, with and without the relaxation of the individual monomers. The basis set superposition error (BSSE) was assessed by the counterpoise (CP) correction introduced by Boys and Bernardi.⁴¹

The relaxed ΔE and ΔE_{BSSE} values are larger by 60 and 59 kJ·mol^{−1}, respectively, for site III than for SII. This can be understood on the basis of the energy necessary for the distortion of the Cu(II) cluster to the corresponding monomeric part within the Cu(II)–C₂H₂ complex. This conclusion is supported by the dramatic geometry change taking place after the adsorption of ethyne on the Cu(II) cluster (compare ref 29 and Figure 3). The Cu(III) cluster, however, remains nearly unmodified in the presence of C₂H₂. Concerning the Cu(III)–C₂H₂ complex, the differences between the values with and without relaxation of the monomers can consequently be traced back, in a good approximation, to the distortion of the ethyne.

The NAO/NBO analysis demonstrates that the bond between ethyne and the individual clusters is due not to covalent interactions but rather to intermolecular donor–acceptor interactions (involving charge transfer from occupied orbitals of one subsystem to unoccupied MOs of the other). Using the sum of the atomic charges of the corresponding monomeric parts allows one to predict a net charge transfer (CT) of 0.14e for Cu(II)–C₂H₂ (0.15e for Cu(III)–C₂H₂) from Cu toward the ethyne, which can be explained predominantly by two synergetic Cu···C₂H₂ interactions. The σ donation emerges from a depletion of one of the two π NBOs (~94% p character) on ethyne by 0.12e for Cu(II)–C₂H₂ (0.13e for Cu(III)–C₂H₂) and a simultaneous occupancy increase of the Cu lone pair of ~97% s* character. The π back-donation results from a depletion of the Cu lone pair of pure d character by 0.23e for Cu(II)–C₂H₂ (0.24e for Cu(III)–C₂H₂) and the corresponding occupancy increase of the π^* NBOs on C₂H₂.

Table 3 summarizes the results of the RVS analysis and the LMP2 correlation energy decomposition in the upper and lower parts, respectively. Besides the SCF interaction energy (E_{INT}), the LMP2 correlation energy (E_{corr}), and the total LMP2 interaction energy (E_{tot}), the sum of all attractive contributions ($\Sigma_{\text{tot, attractive}}$) and the individual terms are given as percentages. Similar to the results in ref 29, the RVS analysis reveals large attractive electrostatic energies (E_{ES}) of comparable magnitude for the two complexes. They are offset by the corresponding exchange repulsion (E_{EXR}) terms.

The electrostatic interaction energies which are steric contributions amount to 51% of all attractive terms in each case. Additional attractive contributions to the total interaction energy (E_{INT}), such as the polarization ($E_{\text{PL(EX)\{A\}}}$ and $E_{\text{PL(EX)\{B\}}}$) and CT energies ($E_{\text{CT(EX)\{A\rightarrow B\}}}$ and $E_{\text{CT(EX)\{B\rightarrow A\}}}$), are orbital contributions. The polarization and, even more, the CT energy of

TABLE 3: Results of the Reduced Variational Space (RVS) Analysis at the RHF Level and of the Local MP2 Correlation Energy Decomposition (LMP2 Part.) for the Cu(II)–C₂H₂ and Cu(III)–C₂H₂ Complexes (Values in kJ·mol⁻¹ and as Percentage of the Sum of All Attractive Terms)

	Cu(II){A}–C ₂ H ₂ {B}			Cu(III){A}–C ₂ H ₂ {B}		
	RVS	LMP2 part.	contr. (%)	RVS	LMP2 part.	contr. (%)
E_{ES}^a	-294.01		51	-301.16		51
E_{EXR}^b	+417.19			+423.59		
$E_{PI(EX)\{A\}}^c$	-32.89		9	-33.93		9
$E_{PI(EX)\{B\}}^c$	-20.13			-20.13		
$E_{CT(EX)\{A\rightarrow B\}}^d$	-65.31		20	-70.42		20
$E_{CT(EX)\{B\rightarrow A\}}^d$	-49.62			-49.50		
E_{BSSE}^e	-1.63			-1.34		
E_{BSSE}^e	-3.89			-3.74		
E_{RES}^f	-13.77			-14.50		
E_{INT}^g	-64.06			-71.87		
E_{disp}^h		-15.35	3		-11.46	2
$E_{ex-disp}^i$		-6.20	1		-6.65	1
E_{ionic}^j		-71.16	12		-73.84	13
$E_{intra-corr}^k$		-25.73	4		-26.25	4
E_{corr}^l		-118.44			-118.20	
E_{tot}^m		-182.50			-190.07	
$\Sigma_{tot,attractive}^n$		-580.40			-593.34	

^a Electrostatic energy. ^b Exchange repulsion energy. ^c Polarization energy of A and B, respectively. ^d Charge transfer from A to B and vice versa. ^e BSSE correction for the CT from A to B and vice versa. ^f Residual terms. ^g Total interaction energy in accordance with the RVS analysis. ^{h-k} Contributions to E_{corr} , the LMP2 correlation energy, due to (h) dispersive coupling, (i) exchange dispersion, (j) ionic excitation, and (k) intramolecular correlation effects. ^l LMP2 correlation contribution to the interaction energy. ^m Total LMP2 interaction energy, $E_{tot} = E_{INT} + E_{corr}$. ⁿ Sum of all attractive contributions except e and f.

both ethyne complexes are characterized by individual components which are distinctly different from those of the corresponding ethene complexes (cf. ref 29); i.e., the ethyne C₂H₂ (fragment {B}) is more strongly polarized by the corresponding fragments {A}, and the charge transfer is unambiguously directed toward the ethyne ({B}) (see the individual contributions in Table 3). These differences are more pronounced for the Cu(III)–C₂H₂ complex, and the slightly larger E_{INT} value of -71.87 kJ·mol⁻¹ can primarily be derived from the more dominant $E_{CT(EX)\{A\rightarrow B\}}$ contribution. The direction of the net charge transfer discovered by the RVS method, i.e., the magnitude of the $E_{CT(EX)\{A\rightarrow B\}}$ value compared to the $E_{CT(EX)\{B\rightarrow A\}}$ contribution, fits excellently to the findings of the NAO/NBO analysis of both ethyne complexes. The polarization of C₂H₂ by the two clusters, and the CT contributions toward the ethyne, are significantly stronger in comparison to those of the ethene complexes.²⁹ On the basis of the RVS analysis applied to the Cu(II)–C₂H₂, the following percentages can be presented as a fraction of their sum: attractive terms E_{ES} , 64%; ($E_{PL(EX)\{A\}}$; $E_{PL(EX)\{B\}}$), (7;4)%; and ($E_{CT(EX)\{A\rightarrow B\}}$; $E_{CT(EX)\{B\rightarrow A\}}$), (14;11)% (the values separated by a semicolon in parentheses distinguish the two entries as defined). The corresponding numbers for the Cu(III)–C₂H₂ complex are 63%, (7;4)%, and (15;11)%.

The LMP2 partitioning of the correlation energy, E_{corr} , renders contributions of the instantaneous CT (E_{ionic}) of 60% (Cu(II)–C₂H₂ complex) and 62% (Cu(III)–C₂H₂) and consequently supports the results of the RVS analysis. The CT contributions amount to a total of 32% and 33% of all attractive terms, respectively; i.e., they are slightly more distinct than for the corresponding ethene adsorption complexes. In comparison to these, the larger individual contributions to the interaction energy, E_{INT} , of the systems studied here and the larger terms

of the instantaneous CT might be explained on the basis of the shorter Cu–C bonds (see section 4.2.1, on Geometries). The closer approach of C₂H₂ obviously enhances the terms E_{ES} and E_{EXR} , which consequently increases the magnitude of the overall polarization and CT effects. Finally, one can conclude that the Cu–zeolite–ethyne interaction energy is dominated by electrostatic and CT contributions, similar to the case for the ethene complexes.

4.2.3. Vibrational Frequency Calculation. One important objective is the investigation of the IR spectra of adsorbed ethyne on vacuum-dehydrated CuNaY by means of harmonic frequency calculations. As we observed two components of the ν_1 , ν_2 , and ν_3 modes of ethyne (see Figure 2 and Table 1), the considerations are limited to the two model systems depicted in Figure 3. This assumption is supported by the results of Maxwell et al.⁴²

Table 1 displays the experimental (ν_{exp}) and calculated harmonic frequencies (ν_{calc}) and frequency shifts ($\Delta\nu_{exp}$ and $\Delta\nu_{calc}$) of ethyne prior to and after adsorption on two different copper sites. The measured shifts are attributed to the different cluster models on the basis of the frequency calculations. It is rewarding that the complex at SIII, which exhibits the larger frequency shift and is predicted to be more strongly bound, is the one which shows up first in the FTIR spectra and acquires more intensity with increasing equilibrium pressure of C₂H₂, demonstrating the higher population of this thermodynamically favored adsorption complex.

The signs of all observed frequency shifts and the magnitudes of the $\Delta\nu_2$ and $\Delta\nu_3$ shifts are correctly reproduced by the calculations, whereas the $\Delta\nu_1$ values of -182/-190 cm⁻¹ are overestimated. However, in contrast to the previous theoretical results of the CC stretching mode of ethene,²⁹ the calculation on the basis of the selected cluster models provides two different vibrational frequencies for the ν_1 CC stretching mode of ethyne in the adsorbed state.

The magnitudes of the calculated shifts to lower wavenumbers demonstrate impressively the important role of the CT predicted by the NAO/NBO analysis and both energy decomposition methods. The population analysis reveals that the σ bonding, and the more pronounced π back-bonding, both weaken the CC bond. Considering the CT term of the RVS analysis, $E_{CT(EX)\{A\rightarrow B\}}$, obviously supports the importance of the back-bonding. This influences most efficiently the ν_1 CC stretching mode, giving rise to the dramatic shifts to lower wavenumbers, which are associated with an elongation of the CC triple bond by 0.03 Å. However, while the calculated $\Delta\nu_2$ and the $\Delta\nu_3$ values agree very satisfactorily with the experimental ones, the predicted $\Delta\nu_1$ values are definitely larger than those observed by 20–30%, most probably due to overestimated CT contributions which lead to too-large interaction energies. Taken into account the experimental precision, this demonstrates the degree of reliability of the present computational methods, possibly attributable to the choice of the model systems.²⁹

5. Conclusions

This paper, continuing our previous investigation dealing with nitrogen and ethene as probe molecules, aims at a characterization of C₂H₂ adsorbed on vacuum-dehydrated CuNaY zeolite. Just like ethene, ethyne is able to distinguish between two chemically inequivalent adsorption sites, as can be derived from two band components for each of the three stretching vibrations. All vibrations, especially the CC stretching mode, are strongly shifted to lower wavenumbers with respect to those found in the gas phase, suggesting pronounced CT effects. The compu-

tational part consists of partial geometry optimizations of two different adsorption complexes and calculations of the interaction energy, as well as their interpretation using the NAO/NBO analysis and energy decomposition methods. Both complexes show nearly planar, four-fold coordination of the copper ion by two oxygen ligands and side-on bound ethyne. Due to the adsorption, the linearity of C_2H_2 is lifted, and the CC bond is elongated by 0.03 Å. The calculated interaction energies, including relaxation, are large and significantly different due to the energy-costly geometry change of the Cu(II) cluster within the Cu(II)– C_2H_2 complex. Population analysis reveals non-Lewis donor–acceptor interactions between the Cu–zeolite and the ethyne, associated with a net charge transfer toward C_2H_2 . The energy decomposition methods at the uncorrelated and correlated levels convincingly support the importance of the electrostatic and CT energies contributing to the overall electronic interaction energy (E_{tot}). Harmonic frequency calculations of the two adsorption complexes were performed in order to relate them to the FTIR experiments. These calculations correctly reproduce the shifts to lower wavenumbers of all stretching vibrations as well as the presence of two band components; however, the calculated $\Delta\nu_1$ shifts of $-182/-190\text{ cm}^{-1}$ are overestimated, possibly due to the artifacts of the selected model systems.

In comparison with the earlier studies of C_2H_2 adsorbed on Brønsted acid sites, the present results reveal a much stronger activation of C_2H_2 by Cu^+ ions attached to the framework of a zeolite, as evidenced by the larger shifts of the bands to lower wavenumbers, a greater elongation of the triple bond, and a much more pronounced charge transfer toward the ethyne. One can assume that this very enhanced activation of *side-on* bound C_2H_2 favors the Diels–Alder reaction of ethyne and 1,3-butadiene, yielding the desired product 1,4-cyclohexadiene. Furthermore, ethyne appears to be more strongly bound and activated than ethene.

Acknowledgment. We are grateful to the CU Chemie Uetikon AG in Switzerland for providing us NaY zeolite.

References and Notes

- (1) Li, Y.; Armor, J. N. *Appl. Catal. B: Environ.* **1992**, *1*, L21.
- (2) Centi, G.; Perathoner, S. *Appl. Catal. A* **1995**, *132*, 179.
- (3) Mizuno, J. W. N.; Misono, M. *Bull. Chem. Soc. Jpn.* **1998**, *71*, 947.
- (4) Shimokawabe, M.; Hirano, K.; Takezawa, N. *Catal. Today* **1998**, *45*, 117.
- (5) Recchia, S.; Dossi, C.; Psaro, R.; Fusi, A.; Ugo, R.; Moretti, G. *J. Phys. Chem. B* **2002**, *106*, 13326.
- (6) Reimlinger, H.; Krücker, U.; de Ruiter, E. *Chem. Ber.* **1970**, *103*, 2317.
- (7) Maxwell, I. E.; Downing, R. S.; van Langen, S. A. *J. Catal.* **1980**, *61*.
- (8) Maxwell, I. E. *Adv. Catal.* **1982**, *31*, 1.
- (9) Dessau, R. M. *J. Chem. Soc., Chem. Commun.* **1986**, 1167.
- (10) Smith, J. V. *Adv. Chem. Ser.* **1971**, *101*, 171.
- (11) Gentry, S. J.; Hurst, N. W.; Jones, A. J. *Chem. Soc., Faraday Trans. 1* **1979**, *75*, 1688.
- (12) Jacobs, P. A.; Beyer, H. K. *J. Phys. Chem.* **1979**, *83*, 1174.
- (13) Liu, S.-B.; Lin, T.-S.; Yang, T.-C.; Chen, T.-H.; Hong, E.-C.; Ryoo, R. *J. Phys. Chem.* **1995**, *99*, 8277.
- (14) Hartmann, M.; Boddenberg, B. *Microporous Mater.* **1994**, *2*, 127.
- (15) Maxwell, I. E.; de Boer, J. J.; Downing, R. S. *J. Catal.* **1980**, *64*, 493.
- (16) Huber, S.; Knözinger, H. *J. Mol. Catal. A: Chem.* **1999**, *141*, 117.
- (17) Knözinger, H.; Huber, S. *J. Chem. Soc., Faraday Trans.* **1998**, *94*, 2047.
- (18) Bordiga, S.; Ricchiardi, G.; Spoto, G.; Scarano, D.; Carnelli, L.; Zecchina, A.; Areán, C. O. *J. Chem. Soc., Faraday Trans.* **1993**, *89*, 1843.
- (19) Onyestyák, G.; Valyon, J.; Rees, L. V. C. *Stud. Surf. Sci. Catal.* **2001**, *135*, 3105.
- (20) de Lara, E. R. C. *Phys. Chem. Chem. Phys.* **1999**, *1*, 501.
- (21) Jang, S. B.; Jeong, M. S.; Kim, Y. *Zeolites* **1997**, *19*, 228.
- (22) Turner, J. F. C.; Benmore, C. J.; Barker, C. M.; Kaltsoyannis, N.; Thomas, J. M.; David, W. I. F.; Catlow, C. R. A. *J. Phys. Chem. B* **2000**, *104*, 7570.
- (23) Evleth, E. M.; Kassab, E.; Jessri, H.; Allavena, M.; Montero, L.; Sierra, L. *J. Phys. Chem.* **1996**, *100*, 11368.
- (24) Ugliengo, P.; Ferrari, A. M.; Zecchina, A.; Garrone, E. *J. Phys. Chem.* **1996**, *100*, 3632.
- (25) O'Malley, P.; Farnworth, K. *J. Phys. Chem. B* **1998**, *102*, 4507.
- (26) Ugliengo, P.; Civalieri, B.; Dovesi, R.; Zicovich-Wilson, C. M. *Phys. Chem. Chem. Phys.* **1999**, *1*, 545.
- (27) Picos, E. A.; West, D. W.; Trifunac, A. D.; Eriksson, L. A. *J. Phys. Chem.* **1996**, *100*, 8408.
- (28) Bonelli, B.; Civalieri, B.; Ugliengo, P.; Gabelica, Z.; Garrone, E. *Phys. Chem. Chem. Phys.* **2002**, *4*, 1658.
- (29) Hübner, G.; Rauhut, G.; Stoll, H.; Roduner, E. *Phys. Chem. Chem. Phys.* **2002**, *4*, 3112.
- (30) Becke, A. D. *J. Chem. Phys.* **1993**, *98*, 5648.
- (31) Frisch, M. J.; Trucks, G. W.; Schlegel, H. B.; Scuseria, G. E.; Robb, M. A.; Cheeseman, J. R.; Zakrzewski, V. G.; Montgomery, J. A., Jr.; Stratmann, R. E.; Burant, J. C.; Dapprich, S.; Millam, J. M.; Daniels, A. D.; Kudin, K. N.; Strain, M. C.; Farkas, O.; Tomasi, J.; Barone, V.; Cossi, M.; Cammi, R.; Mennucci, B.; Pomelli, C.; Adamo, C.; Clifford, S.; Ochterski, J.; Petersson, G. A.; Ayala, P. Y.; Cui, Q.; Morokuma, K.; Malick, D. K.; Rabuck, A. D.; Raghavachari, K.; Foresman, J. B.; Cioslowski, J.; Ortiz, J. V.; Baboul, A. G.; Stefanov, B. B.; Liu, G.; Liashenko, A.; Piskorz, P.; Komaromi, I.; Gomperts, R.; Martin, R. L.; Fox, D. J.; Keith, M. A.; Al-Laham, T.; Peng, C. Y.; Nanayakkara, A.; Gonzalez, C.; Challacombe, M.; Gill, P. M. W.; Johnson, B.; Chen, W.; Wong, M. W.; Andres, J. L.; Gonzalez, C.; Head-Gordon, M.; Replogle, E. S.; Pople, J. A. *Gaussian 98*, Revision A.7; Gaussian, Inc.: Pittsburgh, PA, 1998.
- (32) Reed, A. E.; Curtiss, L. A.; Weinhold, F. *Chem. Rev.* **1988**, *88*, 899.
- (33) Weinhold, F. In *Encyclopedia of Computational Chemistry*; v. Raguè Schleyer, P., Ed.; John Wiley & Sons: Chichester, New York, Weinheim, Brisbane, Singapore, Toronto, 1998; Vol. 3, p 1792.
- (34) Chen, W.; Gordon, M. S. *J. Phys. Chem.* **1996**, *100*, 14316.
- (35) Gordon, M. S.; Jensen, J. H. In *Encyclopedia of Computational Chemistry*; v. Raguè Schleyer, P., Ed.; John Wiley & Sons: Chichester, New York, Weinheim, Brisbane, Singapore, Toronto, 1998; Vol. 5, p 3198.
- (36) Schütz, M.; Rauhut, G.; Werner, H.-J. *J. Phys. Chem. A* **1998**, *102*, 5997.
- (37) Schmidt, M. W.; Baldridge, K. K.; Boatz, J. A.; Elbert, S. T.; Gordon, M. S.; Jensen, J. H.; Koseki, S.; Matsunaga, N.; Nguyen, K. A.; Su, S.; Windus, T. L.; Dupuis, M.; Montgomery, J. A., Jr. *J. Comput. Chem.* **1993**, *14*, 1347.
- (38) MOLPRO is a package of ab initio programs: Werner, H.-J.; Knowles, P. J. (with contributions from Amos, R. D.; Berning, A.; Cooper, D. L.; Deegan, M. J. O.; Dobbyn, A. J.; Eckert, F.; Hampel, C.; Hetzer, G.; Leininger, T.; Lindh, R.; Lloyd, A. W.; Meyer, W.; Mura, M. E.; Nicklass, A.; Palmieri, P.; Peterson, K.; Pitzer, R.; Pulay, P.; Rauhut, G.; Schütz, M.; Stoll, H.; Stone, A. J.; Thorsteinsson, T.) *MOLPRO*, Version 2000.4; University of Birmingham, UK, 1999 (see <http://www.tc.bham.ac.uk/molpro/>).
- (39) Hübner, G.; Roduner, E. *Stud. Surf. Sci. Catal.* **2001**, *135*, 218.
- (40) Herzberg, G. *Molecular Spectra and Molecular Structure, II. Infrared and Raman Spectra of Polyatomic Molecules*; Van Nostrand: Princeton, New York, Toronto, London, 1945.
- (41) Boys, S. F.; Bernardi, F. *Mol. Phys.* **1970**, *19*, 553.
- (42) Maxwell, I. E.; de Boer, J. J.; Downing, R. S. *J. Catal.* **1980**, *61*, 493.
- (43) Weidlein, J.; Müller, U.; Dehnicke, K. *Schwingungsspektroskopie, eine Einführung*; Georg Thieme Verlag: Stuttgart, New York, 1988.